ADVANCED MATERIALS
www.advmat.de

Azo Compounds Derived from Electrochemical Reduction of Nitro Compounds for High Performance Li-Ion Batteries

*Chao Luo, Xiao Ji, Singyuk Hou, Nico Eidson, Xiulin Fan, Yujia Liang, Tao Deng, Jianjun Jiang, and Chunsheng Wang**

Organic compounds are desirable alternatives for sustainable lithium-ion battery electrodes. However, the electrochemical properties of state-of-the-art organic electrodes are still worse than commercial inorganic counterparts. Here, a new chemistry is reported based on the electrochemical conversion of nitro compounds to azo compounds for high performance lithium-ion batteries. 4-Nitrobenzoic acid lithium salt (NBALS) is selected as a model nitro compound to systemically investigate the structure, lithiation/delithiation mechanism, and electrochemical performance of nitro compounds. NBALS delivers an initial capacity of 153 mAh g^{-1} at 0.5 C and retains a capacity of 131 mAh g^{-1} after 100 cycles. Detailed characterizations demonstrate that during initial electrochemical lithiation, the nitro group in crystalline NBALS is irreversibly reduced into an amorphous azo compound. Subsequently, the azo compound is reversibly lithiated/delithiated in the following charge/discharge cycles with high electrochemical performance. The lithiation/delithiation mechanism of azo compounds is also validated by directly using azo compounds as electrode materials, which exhibit similar electrochemical performance to nitro compounds, while having a much higher initial Coulombic efficiency. Therefore, this work proves that nitro compounds can be electrochemically converted to azo compounds for high performance lithium-ion batteries.

Due to the ever-increasing demand for rechargeable lithium-ion batteries (LIBs), environmental benignity and sustainability have become key factors for electrode materials. However, the fabrication of inorganic electrode materials such as $LiCoO_2$ and graphite consumes a huge amount of energy and releases a large amount of CO_2.[1,2] Moreover, the used batteries could trigger more severe environmental problems by leaking toxic heavy metal from cobalt-based electrodes to the soil and water. To circumvent the environmental and sustainability challenges, it is of great importance to develop energy-efficient, sustainable, and recyclable battery materials. Compared to inorganic materials, organic compounds have multiple advantages such as lightweight, abundance, nontoxicity, sustainability, flexibility, and simple structure optimization, which make them promising alternatives to the inorganic counterparts.[3–5] Therefore, replacing inorganic electrodes with organic electrodes in rechargeable batteries is ideal to alleviate the environment and sustainability challenges.

Up to date, four categories of organic molecules, containing disulfide (S—S), organic radicals, carbonyl (C=O) and imine (C=N) functional groups, can function as electrode materials in LIBs (**Scheme 1**). In the first category, the reversible reaction between disulfide compounds and Li-ions depends on the cleavage and regeneration of the disulfide bond. However, it suffers from sluggish reaction kinetics,[6] and the formed thiolate anions are soluble in the electrolyte, resulting in poor cycle stability. In the second category, the organic radicals can reversibly react with Li-ions and various anions (e.g., ClO_4^-, PF_6^-) via n-type and p-type doping mechanisms.[7] Though organic radicals display fast reaction kinetics, the high solubility and self-discharge impedes the practical application of these materials. In the third and fourth categories, the carbonyl or imine compounds can reversibly react with Li-ions through reduction of the carbon-oxygen or carbon-nitrogen double bond to a single bond and triggering intramolecular electron transfer in the conjugated structure. These carbonyl and imine compounds exhibit relatively high specific capacity, thus are the focus of current research in organic electrode materials.[8–25] However, these organic materials are still not competitive with inorganic electrode materials due to their low power density, high time/energy cost for synthesis, and short cycle life induced by their high solubility in organic electrolytes. Hence, it is pivotal to explore new chemistry for organic electrodes with high rate capability, simple synthetic routes, and stable cycle life.

For the first time, we discovered that azo compounds, which can be electrochemically reduced from nitro compounds, are a new family of organic electrode materials with superior electrochemical performance in LIBs. Two nitrobenzoic acid

Dr. C. Luo, X. Ji, S. Hou, N. Eidson, Dr. X. Fan, Y. Liang, T. Deng, Prof. C. Wang
Department of Chemical and Biomolecular Engineering
University of Maryland
College Park, MD 20742, USA
E-mail: cswang@umd.edu
X. Ji, Prof. J. Jiang
School of Optical and Electronic Information
Huazhong University of Science and Technology
Wuhan, Hubei 430074, China
The ORCID identification number(s) for the author(s) of this article can be found under https://doi.org/10.1002/adma.201706498.

DOI: 10.1002/adma.201706498

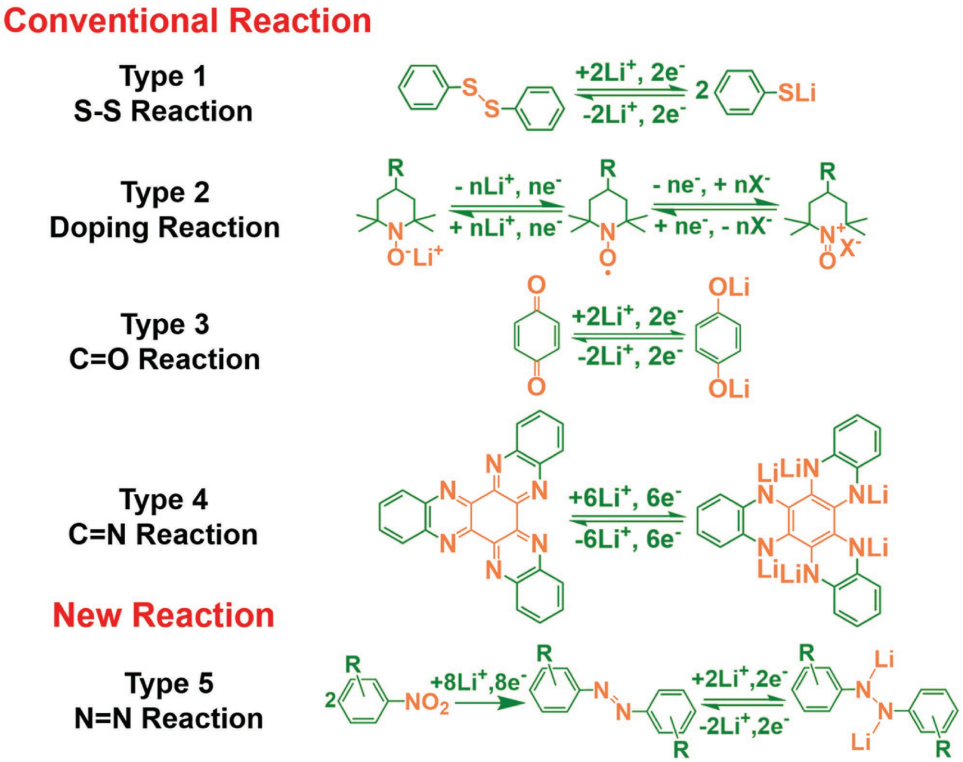

Scheme 1. Working principles of organic molecules in Li-ion batteries. In N=N reaction, two nitro groups are reduced to an azo group by Li-ions, with the formation of Li_2O.

derivatives, 4-nitrobenzoic acid lithium salt (NBALS, **Figure 1**a) and 4-nitrophenylacetic acid lithium salt (NPALS, Figure 1b), were selected as model nitro compounds to evaluate the electrochemical performance as Li-ion battery electrodes. In addition, benzoic acid lithium salt (BALS, Figure 1c), without a nitro group, was used as a control to demonstrate the electrochemical activity of the nitro group. Among them, NBALS exhibits high cycling stability and high rate capability, but a low initial Coulombic efficiency (ICE, 27.3%). The detailed characterizations, using X-ray photoelectron spectroscopy (XPS), Raman spectroscopy, X-ray diffraction (XRD), mass spectrometry, and density functional theory (DFT) calculation, reveal that the low ICE of nitro compounds is attributed to the irreversible reduction of the crystalline nitro compound into an amorphous azo compound during the initial lithiation. The azo compound can reversibly react with Li-ions through the redox reaction of the azo group (N=N). To validate the low ICE mechanism,

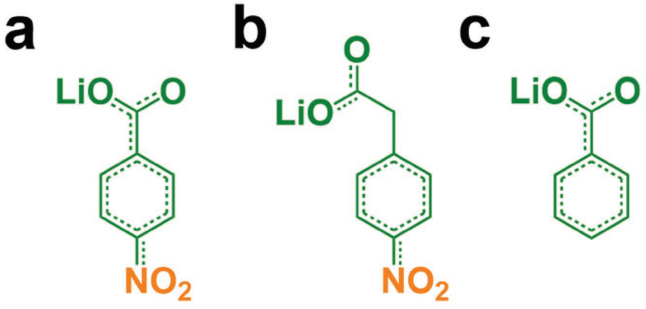

Figure 1. Molecular structure of (a) NBALS, (b) NPALS, and (c) BALS.

4-(phenylazo) benzoic acid lithium salt (PBALS) was directly used as the electrode material. It showed similar electrochemical performance as the nitro compound (NBALS), but with a high ICE (78.9%), confirming that the azo compound is the active electrode material for LIBs. Therefore, this work proves that nitro compounds can be electrochemically converted to azo compounds for high performance LIBs.

Three organic compounds, with a nitro group (NBALS, NPALS) and without a nitro group (BALS), were prepared to investigate the electrochemical activity of a nitro group to Li-ions (Figure 1). The nature of bonding for carbon, oxygen, and nitrogen in these compounds was characterized using XRD, Raman spectroscopy, Fourier transform infrared spectroscopy (FTIR), and XPS. NBALS shows a crystalline structure pattern in XRD (Figure S1a, Supporting Information), and it has typical nitro group vibrations at 1352 cm^{-1} in the Raman spectrum (Figure S1b, Supporting Information) and 1518 cm^{-1} in the FTIR spectrum (Figure S1c, Supporting Information).[26,27] NBALS is stable up to 350 °C as demonstrated by thermal gravimetric analysis (TGA) in Figure S1d in the Supporting Information. The valence states of carbon, oxygen, and nitrogen in NBALS were determined by high resolution XPS (Figure S1e–g, Supporting Information). The elemental C 1s peak at 284.6 eV (Figure S1e, Supporting Information) was used as the reference binding energy. The carbon in the carboxylate group displays a peak at 288.4 eV, which is higher than the peak at 286.0 eV for carbon connected to a nitro group.[28] The increased binding energy for carbon in C—N and C—O is because the electron cloud surrounding the carbon is absorbed by high electronegative atoms such as N and O. The small peak

at 291.0 eV is assigned to a π–π^* shake-up satellite in graphitic carbon.[28] In Figure S1f in the Supporting Information, the oxygens in the carboxylate and nitro groups are represented by two sharp peaks at 531.3 and 532.6 eV, respectively. While in Figure S1g in the Supporting Information, the nitrogen in the nitro group is represented by the strong peak at 405.6 eV, and the weak peak at 406.5 eV is due to the shake-up satellite from the nitro group.[29] The scanning electron microscopy (SEM) image (Figure S1h, Supporting Information) shows that the pristine NBALS consists of microsized particles.

Similarly, NPALS (Figure S2, Supporting Information) and BALS (Figure S3, Supporting Information) were also characterized using XRD, Raman spectroscopy, FTIR, and TGA. Analogous to NBALS, NPALS also has a crystalline structure pattern in XRD (Figure S2a, Supporting Information) and typical nitro group vibrations at 1342 cm^{-1} in the Raman spectrum (Figure S2b, Supporting Information) and 1510 cm^{-1} in the FTIR spectrum (Figure S2c, Supporting Information). The TGA (Figure S2d, Supporting Information) shows that it starts to decompose at a lower temperature of 230 °C. BALS also has a crystalline structure pattern in XRD (Figure S3a, Supporting Information), but obviously it has no nitro group vibration in the Raman or FTIR spectra as expected based on the structure (Figure S3b,c, Supporting Information). BALS is more stable than NBALS and NPALS, with a decomposition temperature of 450 °C.

The electrochemical performance of NBALS, NPALS, and BALS was evaluated in 7 M LiTFSI in 1,3-dioxolane/dimethoxyethane (DOL/DME) electrolyte. **Figure 2** shows the electrochemical behaviors of NBALS. In the first discharge, NBALS exhibits a short and flat plateau at 2.35 V and a long sloping plateau centered at 1.90 V (Figure 2a). A large irreversible capacity with a low ICE of 27.3% is observed in the first charge/discharge. However, in the second cycle, the Coulombic efficiency (CE) increases to >70% and the flat plateau at 2.35 V disappears, while a pair of slopping lithiation/delithiation plateaus at 1.9/2.1 V are still retained. Analogous to galvanostatic charge–discharge curves, the cyclic voltammetry (CV) result shows two cathodic peaks at 2.25 and 2.0 V during the first cathodic scan (Figure 2b), while only one pair of redox peaks is observed in the following scans. In the long-term cycling, NBALS delivers an initial capacity of 153 mAh g^{-1} at 0.5 C (1 C = 155 mA g^{-1}) and retains a capacity of 131 mAh g^{-1} after 100 cycles (Figure 2c). Although NBALS has a large particle size of ≈1 µm, it still shows a very high rate capability with a reversible capacity of 50 mAh g^{-1} even at a high current density of 20 C (Figure 2d). These results prove that nitro compounds show good electrochemical performance in LIBs. To check if the carboxylate group in NBALS participates in the reaction with Li-ions, a methylene group was added between the carboxylate group and benzene ring in NBALS, forming NPALS, where the carboxylate group is no longer conjugated with the aromatic ring (Figure 1). As shown in Figure S4a,b in the Supporting Information, NPALS also exhibits a low ICE (22%) and similar charge/discharge curves as NBALS. The addition of an extra methylene group results in the better lipophilicity of NPALS than NBALS, so the solubility of NPALS in the organic

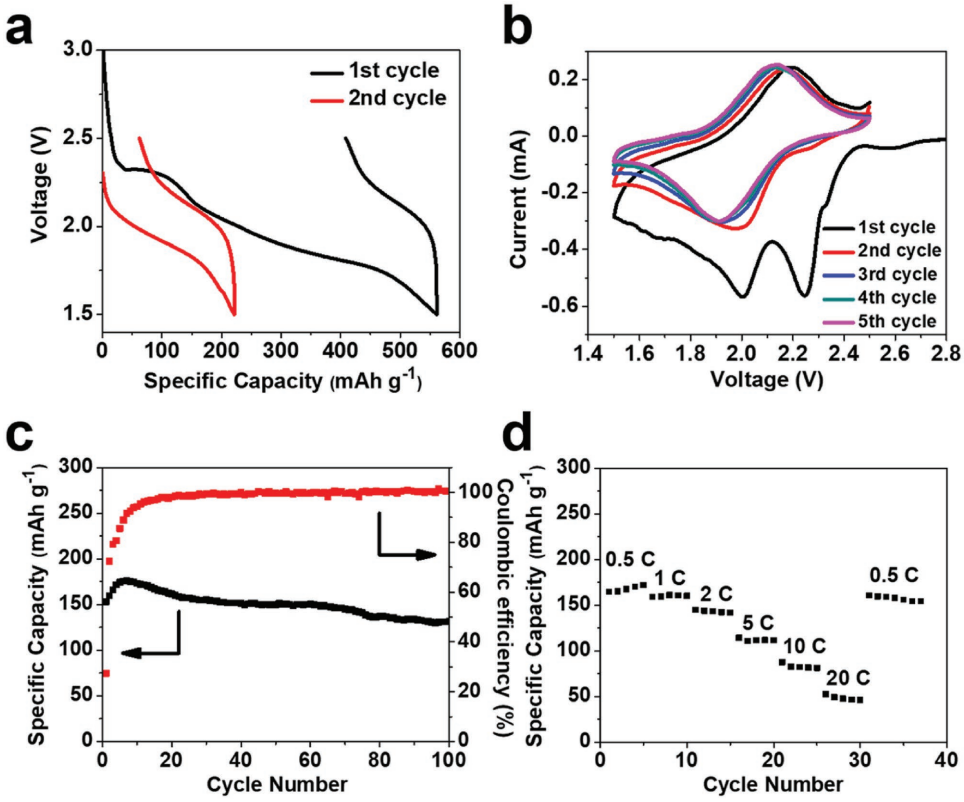

Figure 2. The electrochemical performance of NBALS in Li-ion batteries. a) The galvanostatic charge/discharge curves; b) cyclic voltammograms at 0.1 mV s^{-1}; c) delithiation capacity and Coulombic efficiency versus cycle number at the current density of 0.5 C; d) rate performance at various C-rates.

electrolyte is higher than that of NBALS. The poorer electrochemical behaviors of NPALS than NBALS is most likely due to the high solubility of NPALS in the organic electrolyte. The similar electrochemical behaviors between NPALS and NBALS indicate that the carboxylate group does not participate in the reaction. Moreover, BALS, which only contains a conjugated carboxylate group, shows no electrochemical performance (Figure S4c,d, Supporting Information). Therefore, these results suggest that the nitro group acts as an electrochemically active site in the electrodes for LIBs.

The lithiation/delithiation mechanism of nitro compounds was investigated using XPS. The composition change of the NBALS electrode before and after cycling was also identified by XPS. In the pristine NBALS electrode, carbon and binder were mixed with NBALS powder, so the XPS peaks of pristine NBALS electrode are slightly different from NBALS powder (Figure S1e–g, Supporting Information). The elemental sp^3 C at 284.6 eV (**Figure 3**a,d) was used as the reference binding energy. The three major O 1s peaks at 531.3, 532.7, and 533.1 eV in the NBALS electrode (Figure 3b) represent oxygen from carboxylate, nitro, and hydroxyl groups, respectively. The nitro group comes from the NBALS (Figure S1f, Supporting Information), while the hydroxyl group comes from the sodium alginate binder. The carboxylate group comes from both NBALS and sodium alginate. In the N 1s spectrum (Figure 3c), a strong peak at 405.8 eV represents a nitro group, while two small peaks at 400.1 and 403.3 eV stand for the azo and azoxy groups, respectively (Figure S1g, Supporting Information), which come from the side reaction for the synthesis of NBALS.[30] In the XPS of fully delithiated NBALS after one charge/discharge cycle (Figure 3e), the nitro peak in the O 1s spectrum disappears, while a peak at 530.2 eV for Li_2O shows up. This change in peaks demonstrates that the irreversible reaction between the nitro group and Li-ions occurs during the first cycle. NBALS was cycled from 1.5 to 2.5 V in order to suppress the solid electrolyte interphase (SEI) from forming, and therefore, the Li_2O formed as an irreversible reaction product was not from the SEI.[31] In addition, the nitro peak becomes very weak in the N 1s spectrum of cycled NBALS (Figure 3f), while four peaks at 398.4, 399.9, 401.5, and 403.6 eV, representing a lithiated azo group, an azo group, a nitroso group, and an azoxy group, appear.[28,32] This demonstrates that the irreversible reaction takes place between the nitro group and the Li-ions. XPS analysis demonstrates that NBALS is irreversibly converted to a new azo compound after the initial lithiation/delithiation cycle. Based on the XPS results, the electrochemical reduction mechanism for NBALS in LIBs is proposed in **Scheme 2**. The nitro group in NBALS can successively react with Li-ions to generate an azo compound with a nitroso compound and an azoxy compound as intermediates. Oxygen in the nitro group reacts with Li-ions to generate Li_2O, which has been detected by the XPS O 1s spectrum (Figure 3e). At the same time, nitrogens bond with each other to form azoxy and azo groups, similarly to the chemical reduction of nitro groups by hydrogen. It is well known in catalytic chemistry that nitro compounds can be reduced to aniline by H_2,[33,34] while Li-ions also act as reducing agents to electrochemically reduce nitro compounds to azo compounds. The reversible reaction between azo compounds and Li-ions contributes to the reversible capacity of the NBALS electrode during long-term cycling.

To further confirm the compounds present after the irreversible reaction, Raman spectroscopy, mass spectrometry, XRD and DFT calculations were employed. In **Figure 4**a, the cycled NBALS electrode shows elevated baseline intensity with increased Raman shift, indicating strong fluorescence. The fresh NBALS electrode does not have fluorescence, therefore the fluorescence comes from the product of the irreversible reaction. More importantly, a small peak at 1450 cm^{-1},

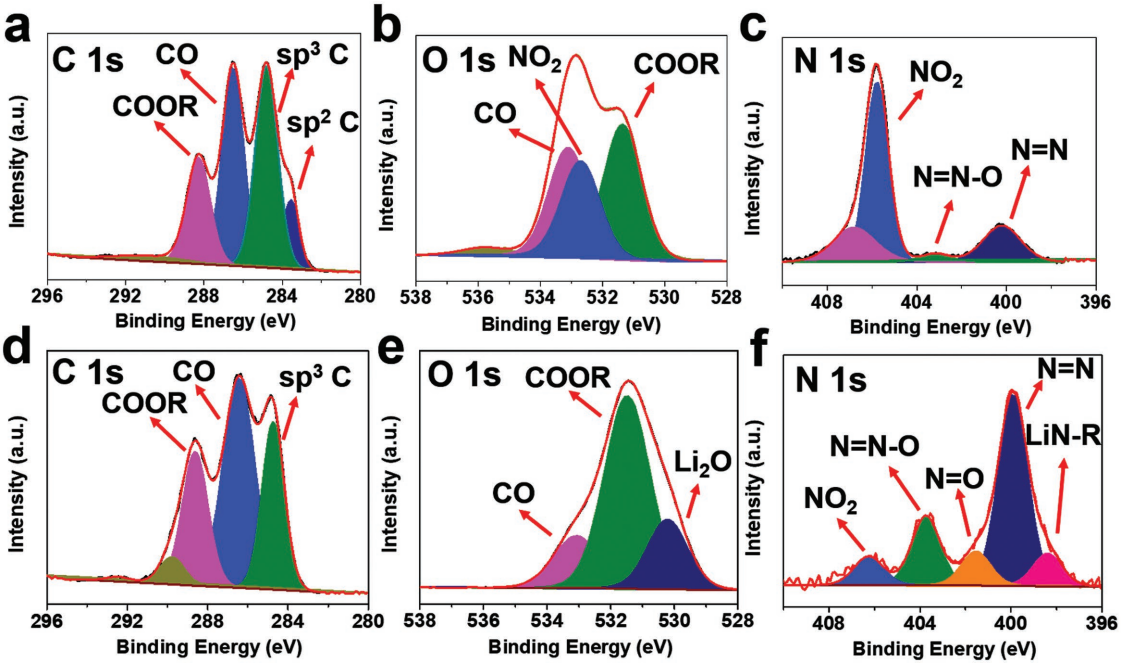

Figure 3. XPS spectra of NBALS electrodes before cycling (a) C 1s, (b) O 1s, and (c) N 1s and after 1 cycle (d) C 1s, (e) O 1s, and (f) N 1s.

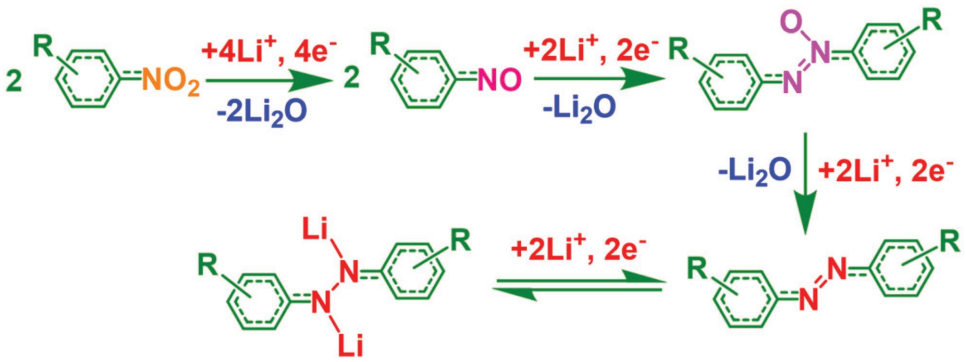

Scheme 2. Reaction mechanism for nitro-based organic materials.

representing an azo group, is observed in the cycled electrode, demonstrating the formation of an azo compound after cycling. In the mass spectra (Figure 4b), the peak at m/z of 165.93 in the pristine NBALS electrode represents the 4-nitrobenzoate anion. After 1 charge/discharge cycle, the peak at m/z of 165.93 is still present. Three other peaks at m/z ratios of 148.90, 268.96, and 284.91 represent 4-nitrosobenzoate anion, azobenzene (AB)-4,4′-dicarboxylate anion, and azoxybenzene-4,4′-dicarboxylate anion, respectively, consistent with the XPS result. All characterizations confirm that the nitro compound is converted to the azo compound after a charge/discharge cycle. XRD was conducted to check the structure of the azo compound in the cycled NBALS. As shown in Figure 4c, the pristine NBALS electrode shows a crystalline structure, while the cycled NBALS electrode becomes amorphous, demonstrating the crystalline NBALS becomes a disordered azo compound after electrochemical reduction by Li-ions. The electrochemical conversion from the nitro compound to the azo compound is further studied by DFT calculation. As shown in Figure 4d, the calculated reaction from the nitro compound to the azo compound occurs at the potential of 2.55 V, which is close to the irreversible reaction plateau at 2.35 V (Figure 2a). Therefore, both experimental and theoretical results confirm that the nitro group acts as an electrochemically active site in LIBs, and an irreversible reaction from the nitro compound to the azo compound occurs in the NBALS electrode.

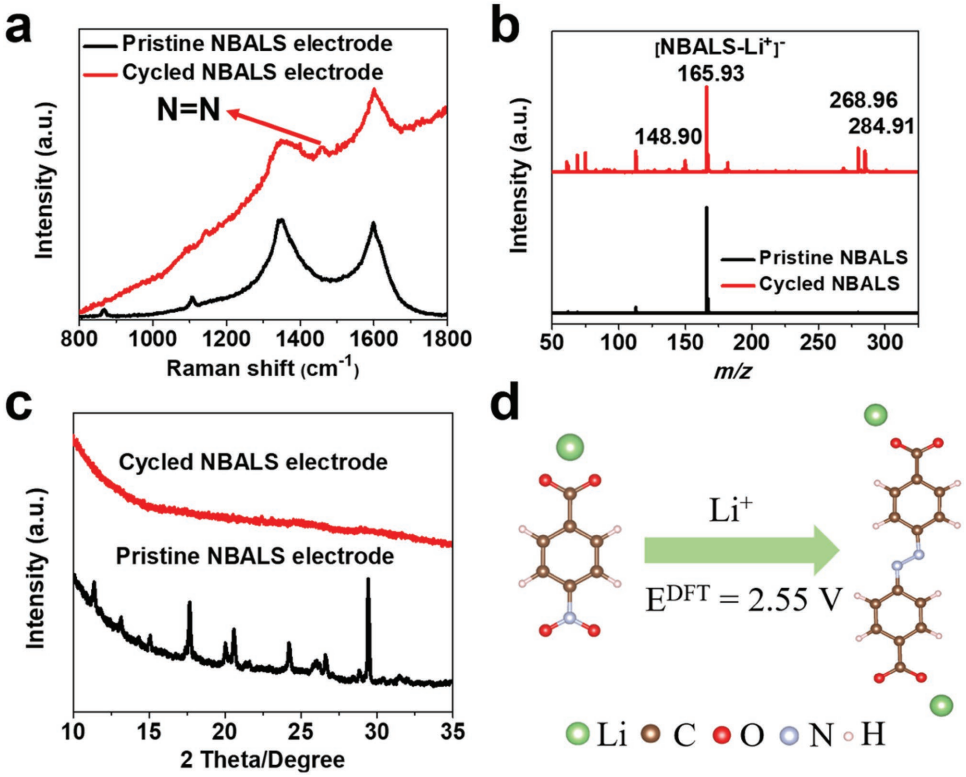

Figure 4. a) Raman spectra of NBALS electrodes before and after 1 cycle; b) mass spectra of NBALS electrodes before and after 1 cycle; c) XRD spectra of NBALS electrodes before and after 1 cycle; d) the illustration and calculated equilibria potential (E^{DFT} vs Li/Li$^+$) for the reduction from NBALS to azo compound.

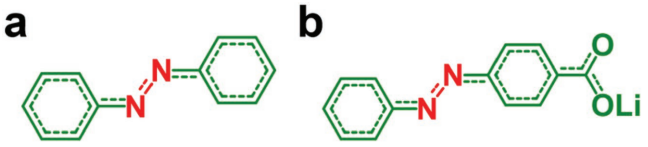

Figure 5. Molecular structure of two simple azo compounds: (a) AB and (b) PBALS.

To further confirm the reaction mechanism, two azo compounds (**Figure 5**), AB and PBALS, were directly used as electrodes for LIBs. AB was used as received, while PBALS was synthesized by neutralizing 4-(phenylazo)benzoic acid with lithium hydroxide. XRD, Raman spectroscopy, FTIR, TGA, and SEM were carried out to characterize PBALS. In Figure S5 in the Supporting Information, PBALS has a crystalline structure with a typical Raman peak for an azo group in the 1400–1450 cm^{-1} range[35] and a typical IR peak for an azo group in the 1575–1630 cm^{-1} range.[36] Moreover, it shows increasing baseline intensity in Raman spectra (Figure S5b, Supporting Information) due to the fluorescence emitted by the azo compound, coinciding with the fluorescent signal in the cycled NBALS electrode (Figure 4a). TGA (Figure S5d, Supporting Information) shows PBALS is stable up to 385 °C. The SEM image in Figure S5e in the Supporting Information shows that the pristine PBALS consists of microsized particles. Therefore, the material characterizations confirm the molecular structure and particle size of PBALS.

The electrochemical performance of AB and PBALS is shown in **Figure 6** and Figure S6 in the Supporting Information. AB exhibits two sloping lithiation plateaus at 2.0 and 1.7 V (Figure S6a, Supporting Information), which are slightly different from one sloping plateau from 2.2 to 1.6 V for NBALS in the second lithiation process (Figure 2a). The difference in lithiation curves is because crystalline NBALS is converted to an amorphous azo compound after one lithiation/delithiation cycle, while AB is in crystalline state. Since AB only contains an azo functional group, the capacity of AB should be provided by the azo group alone. However, AB shows poor cycling stability in Figure S6b in the Supporting Information due to its high solubility in the electrolyte. On the other hand, PBALS, which contains a carboxylate group, shows superior electrochemical performance with an ICE of 78.9%, which is much higher than that (27.3%) of NBALS. In Figure 6a, PBALS shows two discharge plateaus at 1.47 and 1.25 V, and three charge plateaus at 1.30, 1.55, and 2.0 V, corresponding to two cathodic peaks at 1.39 and 1.21 V, and three anodic peaks at 1.33, 1.60, and 1.93 V in the CV (Figure 6b). In the long-term cycling test (Figure 6c), PBALS delivers an initial capacity of 220 mAh g^{-1} at 0.5 C and retains a reversible capacity of 178 mAh g^{-1} after 100 cycles. Moreover, PBALS can retain a reversible capacity of 85 mAh g^{-1} with elevated current density from 0.5 C to 20 C (Figure 6d), indicating its fast charge–discharge behavior even though the particle size is on the microscale (Figure S6e, Supporting Information). Hence, these results prove that azo compounds as a new family of organic electrode materials show

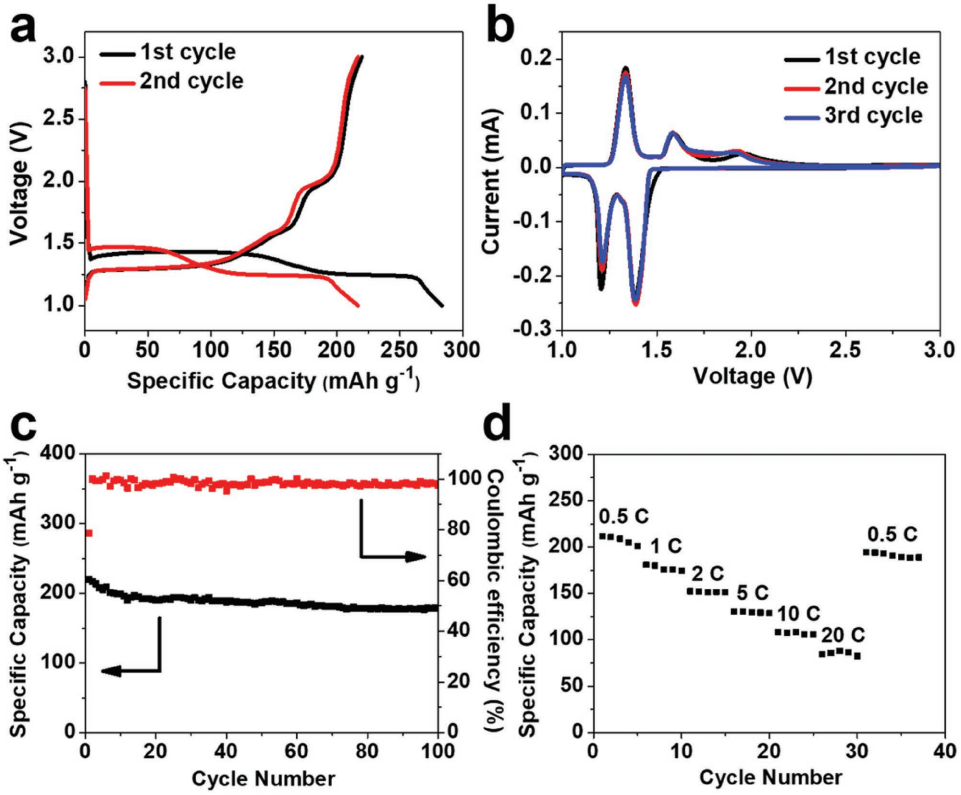

Figure 6. The electrochemical performance of PBALS in Li-ion batteries. a) The galvanostatic charge/discharge curves of PBALS; b) cyclic voltammograms of PBALS at 0.1 mV s^{-1}; c) delithiation capacity and Coulombic efficiency versus cycle number of PBALS at 0.5 C; d) rate performance of PBALS at various C-rates.

superior electrochemical performance in LIBs. The mechanism for high cycling stability of PBALS was investigated using XRD and Raman spectroscopy. Unlike the cycled amorphous NBALS electrode, the PBALS electrode maintains its crystalline structure after cycling (Figure S7a, Supporting Information), demonstrating the lithiation/delithiation of PBALS is reversible. The different crystalline structures between cycled PBALS and NBALS lead to their different charge/discharge behaviors. Similar results were also reported for amorphous and crystalline iron oxide and vanadium oxide.[37,38] The amorphous iron oxide and vanadium oxide show more slopping charge/discharge plateaus than crystalline samples, and the potential of the charge/discharge plateaus of amorphous samples are higher than that of crystalline samples, coinciding with our results. In addition, a redshift in the Raman spectra (Figure S7b, Supporting Information) of the azo peak from 1450 cm^{-1} in the pristine electrode to 1398 cm^{-1} in the cycled electrode at 1 V demonstrates the reaction between the azo group and Li-ions. When PBALS is charged back to 3 V, the azo peak at 1450 cm^{-1} is recovered, confirming the reaction is reversible. Therefore, these results prove that the azo group (N=N) can reversibly react with Li-ions in LIBs.

To understand the high rate capability of nitro and azo compounds, electrochemical impedance spectroscopic evolution of NBALS and PBALS electrodes was measured during charge/discharge cycling. In **Figure 7**a, the interphase resistance of the NBALS electrode, represented by the depressed semi-circle, decreases from ≈130 to ≈110 Ω after 50 cycles due to the lower impedance of the newly formed azo compound. In Figure 7b, the interphase resistance of the PBALS electrode increases from ≈60 to ≈110 Ω after 50 cycles. The low interphase resistance of NBALS and PBALS after cycling enables their fast charge/discharge capability. The reaction kinetics was further studied by conducting CVs for PBALS at various scan rates (Figure 7c). With elevated scan rate, the cathodic peaks shift to lower potentials, while the anodic peaks shift to higher potentials, ascribing to the enhanced polarization. A ln–ln plot of the peak current and scan rate (Figure S8, Supporting Information) shows that the slopes of both anodic and cathodic peaks are close to 0.5, demonstrating the reaction kinetics of PBALS is determined by Li-ion diffusion due to the large particle size (Figure S5e, Supporting Information).[39] The extended π-conjugation in PBALS and strong Li-ion adsorption by nitrogen in the azo group contribute to the fast Li-ion diffusion. To confirm the fast charge/discharge capability and high cyclic stability, the PBALS electrode was cycled at 10 C. It retains a reversible capacity of 95 mAh g^{-1} for 500 cycles with a very slow capacity decay rate of 0.032% per cycle (Figure 7d). Therefore, azo compounds with extended π-conjugation are promising electrode materials for LIBs.

In summary, azo compounds, synthesized from lithiation of nitro compounds, are reported as new Li-ion battery active materials for high performance LIBs. Detailed characterizations demonstrate that during initial lithiation, nitro compounds are irreversibly converted into azo compounds and Li_2O with a low ICE. Then, azo compounds undergo reversible

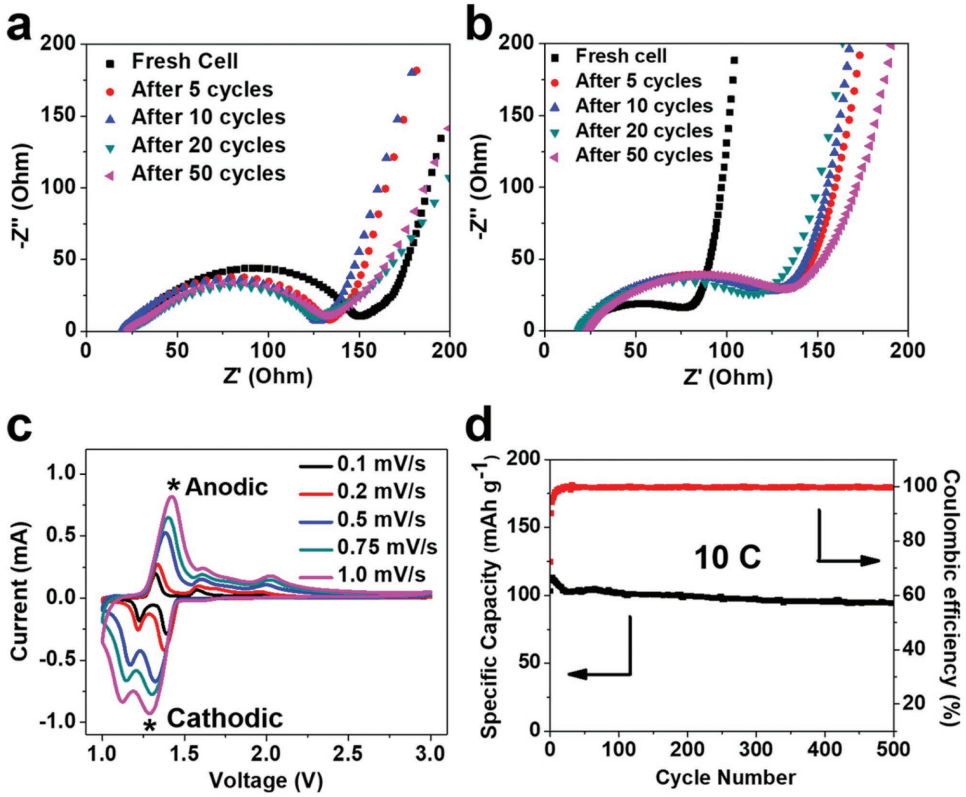

Figure 7. Nyquist plots for (a) NBALS and (b) PBALS cells obtained by electrochemical impedance spectroscopy (EIS) tests before and after cycling at fully charged states. c) CV curves of PBALS at various scan rates and the ln relationship of peak current and scan rate in the insert. d) Delithiation capacity and Coulombic efficiency versus cycle number of PBALS at 10 C.

lithiation/delithiation in the following charge/discharge cycles with high Coulombic efficiency. Both the nitro compound (NBALS) and the azo compound (PBALS) show good cycling stability and high rate capability, while NBALS has a lower ICE (27.3%) than PBALS (78.9%), which is consistent with the reaction mechanism of nitro compounds. The superior electrochemical performance of NBALS and PBALS makes them promising organic electrode materials for sustainable LIBs. The discovery of nitro and azo compounds for organic electrodes offers new opportunities for high performance LIBs.

Experimental Section

Material Synthesis: Nitrophenylacetic acid, 4-nitrobenzoic acid, benzoic acid, AB, and 4-(phenylazo)benzoic acid were purchased from Sigma-Aldrich and used as received.[40] NPALS and PBALS were prepared as follows: nitrophenylacetic acid or 4-(phenylazo)benzoic acid was dispersed in ethanol with 5% excess lithium hydroxide. The solution was stirred at room temperature for 24 h and then filtered to collect the precipitate. The precipitate (NPALS/PBALS) was washed with ethanol and dried in a vacuum oven at 100 °C overnight. NBALS and BALS were prepared as follow: 4-nitrobenzoic acid or benzoic acid was dissolved in ethanol with lithium hydroxide in a 1:1 molar ratio. The solution was stirred at room temperature for 24 h and then heated to 60 °C to remove the ethanol. The white powder (NBALS/BALS) was collected and dried in a vacuum oven at 100 °C overnight. All the materials were analyzed by mass spectrometry in Figure S9 in the Supporting Information.

Material Characterizations: SEM images were taken by a Hitachi SU-70 analytical ultrahigh resolution SEM (Japan). XRD patterns were recorded with a Bruker Smart1000 (Bruker AXS Inc., USA) using a CuK_α radiation source. Raman measurements were performed on a Horiba Jobin Yvon Labram Aramis using a 532 nm diode-pumped solid-state laser, attenuated to give ≈900 µW power at the sample surface. Fourier transform infrared spectra (FTIR) were recorded on a NEXUS 670 FTIR Instrument. Mass spectra utilized anions of the salts produced by an electrospray ionization time of flight mass spectrometer (AccuTOF, JEOL, USA, Inc.). Mass spectra were acquired under negative mode with the following parameters: capillary voltage, 2100 V; orifice 1 voltage, 20 V; orifice 2 voltage, 5 V; ring voltage, 5 V; and dissolution temperature 100 °C. XPS data were collected on a Kratos Axis 165 X-ray photoelectron spectrometer operating in hybrid mode using a monochromatic Al Kα (1486.7 eV) X-rays. High resolution data were collected at a pass energy of 40 eV and charge neutralization was required to minimize sample charging. XPS data were analyzed using CasaXPS software, using peaks with a 70% Gaussian/30% Lorentzian peak shape after subtraction of a Shirley background.

Electrochemical Measurements: The organic compounds were mixed with carbon black and sodium alginate binder to form a slurry at the weight ratio of 60:30:10 (polyvinylidene fluoride (PVDF) binder is used for electrodes using AB due to its strong hydrophobic property). The electrode was prepared by casting the slurry onto aluminum foil using a doctor blade and dried in a vacuum oven at 100 °C overnight (electrodes using AB were dried at 60 °C overnight due to its low melting point). The slurry coated on aluminum foil was punched into circular electrodes with an area mass loading of ≈1.5 mg cm^{-2}. The thickness of the electrode is ≈30 µm (Figure S10, Supporting Information). Coin cells for LIBs were assembled with lithium metal as the counter electrode, 7 M lithium bis(trifluoromethane)sulfonimide (LiTFSI) in a mixture of DOL/DME (1:1 by volume) as the electrolyte, and Celgard3501 (Celgard, LLC Corp., USA) as the separator. Electrochemical performance was tested using an Arbin battery test station (BT2000, Arbin Instruments, USA). Cyclic voltammograms were recorded using a Gamry Reference 3000 Potentiostat/Galvanostat/zero-resistance ammeter (ZRA) with a scan rate of 0.1 mV s^{-1}. Impedance analysis was also performed using a Gamry Reference 3000 Potentiostat/Galvanostat/ZRA.

Supporting Information

Supporting Information is available from the Wiley Online Library or from the author.

Acknowledgements

This work was supported by the US National Science Foundation (NSF) Award No. 1438198. The authors acknowledge the support of the Maryland NanoCenter and its NispLab. The NispLab was supported in part by the NSF as a Materials Research Science and Engineering Center (MRSEC) Shared Experimental Facility.

Conflict of Interest

The authors declare no conflict of interest.

Keywords

azo compound, electrochemical conversion, lithium-ion batteries, nitro compound, organic electrode materials

Received: November 7, 2017
Revised: February 23, 2018
Published online:

[1] C. P. Grey, J. M. Tarascon, *Nat. Mater.* **2016**, *16*, 45.
[2] D. Larcher, J.-M. Tarascon, *Nat. Chem.* **2014**, *7*, 19.
[3] Y. Xu, M. Zhou, Y. Lei, *Mater. Today* **2018**, *21*, 60.
[4] S. Muench, A. Wild, C. Friebe, B. Häupler, T. Janoschka, U. S. Schubert, *Chem. Rev.* **2016**, *116*, 9438.
[5] Y. Liang, Z. Tao, J. Chen, *Adv. Energy Mater.* **2012**, *2*, 742.
[6] B. Häupler, A. Wild, U. S. Schubert, *Adv. Energy Mater.* **2015**, *5*, 1402034.
[7] Z. Song, H. Zhou, *Energy Environ. Sci.* **2013**, *6*, 2280.
[8] M. Armand, S. Grugeon, H. Vezin, S. Laruelle, P. Ribière, P. Poizot, J.-M. Tarascon, *Nat. Mater.* **2009**, *8*, 120.
[9] Y. Morita, S. Nishida, T. Murata, M. Moriguchi, A. Ueda, M. Satoh, K. Arifuku, K. Sato, T. Takui, *Nat. Mater.* **2011**, *10*, 947.
[10] Y. Liang, Y. Jing, S. Gheytani, K.-Y. Lee, P. Liu, A. Facchetti, Y. Yao, *Nat. Mater.* **2017**, *16*, 841.
[11] Y.-L. Wu, N. E. Horwitz, K.-S. Chen, D. A. Gomez-Gualdron, N. S. Luu, L. Ma, T. C. Wang, M. C. Hersam, J. T. Hupp, O. K. Farha, R. Q. Snurr, M. R. Wasielewski, *Nat. Chem.* **2016**, *9*, 466.
[12] H. Chen, M. Armand, M. Courty, M. Jiang, C. P. Grey, F. Dolhem, J. M. Tarascon, P. Poizot, *J. Am. Chem. Soc.* **2009**, *131*, 8984.
[13] C. Luo, R. Huang, R. Kevorkyants, M. Pavanello, H. He, C. Wang, *Nano Lett.* **2014**, *14*, 1596.
[14] X. Han, C. Chang, L. Yuan, T. Sun, J. Sun, *Adv. Mater.* **2007**, *19*, 1616.
[15] Z. Song, H. Zhan, Y. Zhou, *Angew. Chem., Int. Ed.* **2010**, *49*, 8444.
[16] Y. Liang, P. Zhang, S. Yang, Z. Tao, J. Chen, *Adv. Energy Mater.* **2013**, *3*, 600.
[17] T. Nokami, T. Matsuo, Y. Inatomi, N. Hojo, T. Tsukagoshi, H. Yoshizawa, A. Shimizu, H. Kuramoto, K. Komae, H. Tsuyama, J. I. Yoshida, *J. Am. Chem. Soc.* **2012**, *134*, 19694.
[18] Z. Song, Y. Qian, M. L. Gordin, D. Tang, T. Xu, M. Otani, H. Zhan, H. Zhou, D. Wang, *Angew. Chem., Int. Ed.* **2015**, *54*, 13947.
[19] M. Park, D. S. Shin, J. Ryu, M. Choi, N. Park, S. Y. Hong, J. Cho, *Adv. Mater.* **2015**, *27*, 5141.

[20] S. Wang, L. Wang, K. Zhang, Z. Zhu, Z. Tao, J. Chen, *Nano Lett.* **2013**, *13*, 4404.
[21] M. Lee, J. Hong, D. H. Seo, D. H. Nam, K. T. Nam, K. Kang, C. B. Park, *Angew. Chem., Int. Ed.* **2013**, *52*, 8322.
[22] J. Hong, M. Lee, B. Lee, D.-H. Seo, C. B. Park, K. Kang, *Nat. Commun.* **2014**, *5*, 5335.
[23] C. Peng, G.-H. Ning, J. Su, G. Zhong, W. Tang, B. Tian, C. Su, D. Yu, L. Zu, J. Yang, M.-F. Ng, Y.-S. Hu, Y. Yang, M. Armand, K. P. Loh, *Nat. Energy* **2017**, *2*, 17074.
[24] M. Lee, J. Hong, B. Lee, K. Ku, S. Lee, C. B. Park, K. Kang, *Green Chem.* **2017**, *19*, 2980.
[25] M. Kolek, F. Otteny, P. Schmidt, C. Mück-Lichtenfeld, C. Einholz, J. Becking, E. Schleicher, M. Winter, P. Bieker, B. Esser, *Energy Environ. Sci.* **2017**, *10*, 2334.
[26] I. R. Lewis, N. W. Daniel, P. R. Griffiths, *Appl. Spectrosc.* **1997**, *51*, 1854.
[27] M. Arivazhagan, S. Jeyavijayan, *Indian J. Pure Appl. Phys.* **2011**, *49*, 516.
[28] F. Tian, Y. Cui, A. V. Teplyakov, *J. Phys. Chem. C* **2014**, *118*, 502.
[29] G. Distefano, M. Guerra, F. P. Colonna, D. Jones, G. Consiglio, D. Spinelli, *Chem. Phys.* **1982**, *72*, 267.
[30] E. R. Kenawy, E. S. Aly, F. I. Abdel-Hay, R. Abdeen, Y. A. G. Mahmoud, *J. Saudi Chem. Soc.* **2011**, *15*, 327.
[31] K. Xu, *Chem. Rev.* **2014**, *114*, 11503.
[32] Y. Xu, Z. Li, F. Zhang, X. Zhuang, Z. Zeng, J. Wei, *RSC Adv.* **2016**, *6*, 30048.
[33] A. Corma, P. Concepción, P. Serna, *Angew. Chem., Int. Ed.* **2007**, *46*, 7266.
[34] E. A. Gelder, S. D. Jackson, C. M. Lok, *Chem. Commun.* **2005**, 522.
[35] M. M. J. Tecklenburg, D. J. Kosnak, A. Bhatnagar, D. K. Mohanty, *J. Raman Spectrosc.* **1997**, *28*, 755.
[36] I. A. Mohammed, A. Mohammed, *Molecules* **2010**, *15*, 7498.
[37] S. A. Pervez, D. Kim, U. Farooq, A. Yaqub, J. Choi, Y. Lee, C. Doh, *ACS Appl. Mater. Interfaces* **2014**, *6*, 11219.
[38] F. Mattelaer, K. Geryl, G. Rampelberg, J. Dendooven, C. Detavernier, *ACS Appl. Mater. Interfaces* **2017**, *9*, 13121.
[39] V. Augustyn, J. Come, M. A. Lowe, J. W. Kim, P.-L. Taberna, S. H. Tolbert, H. D. Abruña, P. Simon, B. Dunn, *Nat. Mater.* **2013**, *12*, 518.
[40] E. Merino, *Chem. Soc. Rev.* **2011**, *40*, 3835.